

Quantitative Aspects, Engineering and Optimization of Bacterial Sensor Systems

Florian Anderl, *Student Member, IEEE*, Gabriela Salvadori, Mladen Veletic, Fernanda Cristina Petersen and Ilangko Balasingham, *Senior Member, IEEE*

Abstract—Bacterial sensor systems can be used for the detection and measurement of molecular signal concentrations. The dynamics of the sensor directly depend on the biological properties of the bacterial sensor cells; manipulation of these features in the wet lab enables the engineering and optimization of the bacterial sensor kinetics. This necessitates the development of biologically meaningful computational models for bacterial sensors comprising a variety of different molecular mechanisms, which further facilitates a systematic and quantitative evaluation of optimization strategies. In this work, we dissect the detection chain of bacterial sensors from a mathematical perspective from which we derive, supported by wet-lab data, a complete computational model for a *Streptococcus mutans*-based bacterial sensor as a case example. We address the engineering of bacterial sensors by investigating the impact of altered bacterial cell properties on the sensor response characteristics, specifically *sensor sensitivity* and *response signal intensity*. This is achieved through a sensitivity analysis targeting both the steady-state and transient sensor response characteristics. Alongside the demonstration of suitability of our methodological approach, our analysis shows that an increase of sensor sensitivity, through a targeted manipulation of bacterial physiology, often comes at the cost of generally diminished sensor response intensity.

Index Terms—Bacterial Sensor, Molecular Communication, Biochemical Systems Theory, Sensitivity Analysis

I. INTRODUCTION

MOLECULAR Communication (MC) is a biology-inspired communications paradigm that is based on the notion of information encoded onto molecular carriers [1]. It is believed to possess vast potential to revolutionize the health care field and much initial research is conducted to explore its capabilities [2]. MC is the basis for the envisioned *Internet of Bio-Nano Things* (IoBNT) in which bio-nanomachines are connected in networks and exchange information over an MC link [3]. IoBNT plays a crucial role in the future of theranostics in form of implantable bio-nanosensors (BNS) continuously screening health-relevant parameters and communicating this data in real-time over radio links to a hub which could be connected to the Internet. A conceivable application is, for example, the early-detection of bacterial or viral infections where molecular markers of an ongoing infection are detected.

Florian Anderl is with the Department of Electronic Systems, Norwegian University of Science and Technology, 7491 Trondheim, Norway.

Gabriela Salvadori is with the Intervention Centre, Oslo University Hospital, 0424 Oslo, Norway

Mladen Veletic and Ilangko Balasingham are with the Intervention Centre, Oslo University Hospital, 0424 Oslo, Norway, and also with the Department of Electronic Systems, Norwegian University of Science and Technology, 7491 Trondheim, Norway.

Fernanda Cristina Petersen is with the Institute of Oral Biology, Faculty of Dentistry, University of Oslo, 0317 Oslo, Norway

Much of research in MC either focuses on the theoretical implications of MC systems and networks [4]–[7] or quantitative information extraction from biological systems [8], [9]. As MC ultimately aims at engineering and prototyping practical solutions, selected works study feasible MC components. The survey [10], for example, explores the requirements, communication-theoretic properties and possible architectures for MC transmitter (Tx) and receiver (Rx) components. It distinguishes between two main classes of conceivable architectures: nanomaterial-based and biology-based designs. An example for the former category is the graphene-based bioFET MC receiver design [11]. In contrast, the latter category leverages synthetic biological elements, e.g., human or bacteria cells that can be genetically engineered for a specific purpose. Here, bacteria are especially relevant due to the relative ease of genetically engineering them for specific purposes which make bacteria invaluable for various scientific, health-care related and industrial applications.

Consequently, MC has acknowledged this potential in several works. Examples include a concept where engineered bacteria are repurposed as transceivers with different operational modes in an MC link [12]. Moreover, an MC architecture with proton pumping bacteria was recently investigated [13], and a bacterial receiver prototype using the rhamnose operon in a microfluidic environment was presented alongside a computational model [14].

MC borrows the utility of bacteria as receivers from a key area of application for synthetic bacteria: the *sensing* of analytes. The deployment of bacteria as biosensors for a variety of substances is a well-researched field in microbiology and bio-engineering. Many works explore the principles and techniques for engineering bacterial biosensors [15]–[17], and investigate various areas of applications for bacterial biosensors, from environmental monitoring [18]–[20] to medical applications [21]–[25].

While much of the related literature describes a more qualitative approach, only few works attempt to derive quantitative measures for bacterial biosensors [26]. Numerous computational models for dynamics arising from specific bacterial mechanisms have been published [27]–[32]. Nevertheless, to the knowledge of the authors none addresses the general dynamics of bacterial systems with focus on its sensor properties. A lack of a computational framework that describes the sensing dynamics of bacterial sensors prevents us from proceeding with a systematic investigation of how the dynamics can be altered to adhere to specific requirements of the engineered bacterial sensor.

Most conceivable bacterial biosensors rely on the same key processes and biochemical principles and thus have similar structures. This similarity is useful for a computational analysis of these key processes and the resulting qualitative and quantitative dynamics of bacterial sensors in general. This analysis further allows for a systematic investigation of how these dynamics can be altered to adhere to specific requirements on the bacterial sensor. In this paper, we therefore conduct a computational analysis of bacterial sensors and how bacteria can be engineered and optimized catering to the requirements of building actual bacteria-based components for MC. We examine the general components, integral features and critical processes of bacterial sensors with an emphasis on sensing and detection. Through this, we summarize the mechanisms that underlie general bacterial sensors and derive corresponding mathematical models. Using methods from biochemical systems theory (BST) we analyze the steady-state and transient dynamics of a *generic* bacterial sensor. We then proceed to derive expressions for the sensitivity and signal intensity of the sensor. For these measures we then conduct a sensitivity analysis and thereby identify critical parameters of the model and quantify how changes in these affect the model dynamics. For example, similar to an antenna in a telecommunications link or a radar dish, a bacteria-based MC sensor- or receiver should exhibit a measure for gain.

As a case study, we present a concrete example of utilizing the proposed general computational framework for building a computational model for analyzing a bacterial sensor based on experimentation with the bacterial species *Streptococcus mutans*. As basis for a reporter, we use the *luc* gene encoding the enzyme luciferase from the firefly *Photinus pyralis* firefly (further referred to as *lucFF*), which is inserted into the genome of a bacterial sensor strain. These modified bacteria produce the luciferase enzyme, which upon addition of luciferin results in the emission of a light signal proportional to a chemical target signal, functioning as sensors. This allows, for instance, integration with a photodetector which further facilitates integration with electronic elements.

The remainder of the paper is structured as follows. Sec. II discusses important aspects of bacteria as biosensors and presents necessary biological background information. Sec. III provides the theoretical framework which we employ for our analysis. Sec. IV analyzes the discrete processes in a bacterial sensor and summarizes mathematical modeling approaches for the mechanisms. In Sec. V, we then present a mathematical model for a *Streptococcus mutans*-based sensing system and compare this model to our empirical wet-lab data. Sec. VI presents a systematic scheme for analyzing a bacterial sensor's performance. Based on this, we comment on strategies for optimization of bacterial sensors. Finally, Sec. VII concludes the paper and outlines potential research building on this work.

II. BACTERIA AS BIOSENSORS

The general structure of a bacterial sensor is depicted in Fig. 1. The bacteria's molecular response pathway is activated by a target analyte or effector eliciting the expression of reporter genes which, in the genome, are inserted downstream

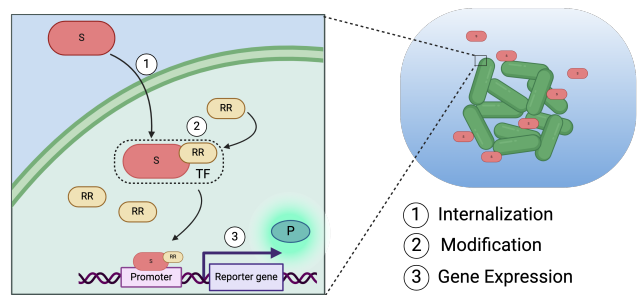


Figure 1. Overview of general bacterial sensor mechanism. Molecular signal S, response regulator RR, transcription factor TF and reporter P. (Illustration was created with *BioRender.com*).

of the regulated primary gene. The reporter proteins resulting from this gene expression or rather their specific activity then are a proxy for the analyte concentration. This mechanism is governed by several distinct sub-processes emphasized in Fig. 1: *internalization*, *modification* and *gene expression*.

Internalization describes the uptake process of the extracellular signal into the sensing cell either directly or by effect as is the case in, for example, phosphorylation. In this case, the external signal binds to receptors on the cell surface which elicits a response inside the cell. Subsequent to uptake, the internalized analyte may undergo several modification steps involving a *response regulator* (RR). Finally, the resulting *transcription factor* (TF) then regulates gene expression. These processes are detailed further below in Sec. IV.

Various reporter mechanisms exist, most prominently: colorimetry, fluorescence (FL) and bioluminescence (BL). Colorimetry is based on assay color changing reactions elicited by, for example, beta-galactosidase resulting from the expression of the *lacZ* reporter gene. FL and BL rely on chemical reactions producing light at specific wavelengths. FL resulting from expression of genes like *gfp*, *egfp* or *mCherry* requires excitation from an external light source. In contrast, BL functions without external activation which makes it especially relevant for applications in which the bacterial sensor component is integrated into an electronic device. The most important BL reporter proteins are the bacterial luciferase variants LuxAB, LuxCDABE and firefly luciferase LucFF. Various aspects influence the choice of reporter protein: substrate availability (for example, BL relies on oxygen and luciferin), sensitivity and, crucially, harvestability. A comprehensive overview of reporters is given in [15].

We further distinguish between single-cell and population-based bacterial sensors. The former exhibits a cellular granularity since the response of single cells is considered [33], [34]. In contrast, in the population-based approach the response of the entire population of the sensing strain is measured. The stochasticity inherent in molecular mechanisms (especially relevant at low analyte concentrations) and gene expression results in generally non-deterministic single-cell bacterial sensor dynamics. This implies heterogeneous reporter expression levels across a sensor population. This heterogeneity can be measured through microscopy imaging and be advantageous for certain sensing applications as it can potentially resolve

spatial information.

In this paper, we restrict our treatment to an analysis of whole-cell bacterial sensors on population-basis deployed in an aqueous assay. This implies a homogeneous concentration of a target analyte in the assay and each viable bacterial cell being exposed to the same concentration of target analyte. We assume further that each viable bacterial cell contributes equally to the overall sensor response, i.e., we ignore the natural heterogeneity of gene expression across a bacterial population. We justify this by our aiming at deriving a model for the *mean bacterial cell response*, as discussed in Sec. V-C.

We further distinguish between two general sensing scenarios:

a) *Scenario 1 - Abundance of Analyte*: In this case, the analyte concentration in the sensing cavity is sufficiently high so that it is not influenced or noticeably diminished by the sensor dynamics itself. This could be the case if there exists a constant supply of analyte into the sensing cavity which is a reasonable assumption for cases of e.g., acute infection with a virulent bacterial strain that is in the stationary phase of its growth cycle. If the virulent strain emits a specific detectable signal (e.g., through *Quorum Sensing*), we can assume an abundant signal supply. In this case, the target analyte enters the computational model describing the sensor as *constant independent variable*. As a result, a bacterial sensor cell reaches a non-zero steady-state response level.

b) *Scenario 2 - Scarcity of Analyte*: When the effector signal is at a low concentration and depleted without experiencing a positive influx it must be included in the computational model as an additional equation as the bacterial sensor *itself* affects the concentration of analyte.

In Sec. VI, we use *Scenario 1* and *Scenario 2* for a systematic steady-state and dynamic optimization analysis, respectively.

III. THEORETICAL FRAMEWORK

Bacterial sensors can be analyzed as biochemical systems at different levels of abstraction. Low concentrations of involved biochemical species mandate stochastic and particle-based models accounting for the probabilistic nature of molecular interactions. Monte-Carlo simulations allow for the synthesis of deterministic trajectories from the stochastic models. Alternatively, direct deterministic models based on reaction-rate equations (RREs) are often a simpler approach while retaining the capability of capturing the system dynamics accurately.

In this section, we give a brief overview of BST as it provides methods that are crucial for our analysis of a bacterial sensor. In the following section, we then outline dynamics of various bacterial sensors and subsequently apply the BST methodology to the derived models of bacterial sensors to provide a systematic analysis of their performance, thus revealing potential starting points for their optimization.

A. Biochemical Systems Theory

BST studies methods for mathematical modeling of biochemical systems [35]. It does so by deriving simplistic approximative models that allow for facilitated mathematical

analysis while retaining the dynamics observed in the data. The analysis of a biochemical system generally begins with the identification of structural relationships in the studied system which can be comprehensively illustrated by graphical representations (as done in Sec. IV, cf. Fig. 2). The dynamics of a system with various constituent species X_1, X_2, \dots, X_n are generally described by a set of ordinary-differential-equations (ODEs) parametrized by $\Theta_R = \{\theta_1, \dots, \theta_F\}$ as

$$\begin{aligned} \dot{X}_1 &= v_1^+(X_1, \dots, X_n, \dots, X_{n+m}; \Theta_R) \\ &\vdots \\ &\quad - v_1^-(X_1, \dots, X_n, \dots, X_{n+m}; \Theta_R) \\ \dot{X}_n &= v_n^+(X_1, \dots, X_n, \dots, X_{n+m}; \Theta_R) \\ &\quad - v_n^-(X_1, \dots, X_n, \dots, X_{n+m}; \Theta_R) \end{aligned} \quad (1)$$

where the flux terms $v_i^{+/-}$, $i = 1, \dots, n$ are either positive fluxes adding to a pool of species X_i or negative when depleting it. These fluxes are in general functions of the system's n internal state variables $\mathbf{X}_{\text{int}} = [X_1, \dots, X_n]^T$ and m external variables $\mathbf{X}_{\text{ext}} = [X_{n+1}, \dots, X_{n+m}]^T$. The fluxes specifically depend on a subset of variables identified in the structural analysis of the biochemical system under investigation. The flux terms can assume various different functional forms: from basic RREs to terms describing complex mechanisms as, for example, *Michaelis-Menten-kinetics* or *Competitive Inhibition*.

It is mathematically convenient to employ an universal form for representing the fluxes $v_i^{+/-}$ regardless of the dynamics governing the specific case and this form is provided by the *Power-Law-Formalism*. As in a classical mass-action derived RRE, a single flux is modeled as a product of a kinetic rate constant γ and involved species among which each are raised to a power of a specific kinetic rate (or kinetic orders) f , i.e.,

$$v_i^{+/-} = \gamma_i \prod_{j=0}^{n+m} X_j^{f_{ij}}, \quad i = 1, \dots, n. \quad (2)$$

In (1), a flux $v_i^{+/-}$ can consist of several distinct processes (chemical reactions, molecular interactions, etc.), i.e., $v_i^{+/-} = \sum_{k=1}^{T_i} v_{ki}^{+/-}$. The choice of representing a biochemical system with aggregated flux terms $v_i^{+/-}$ or, alternatively, distinguishing single process rates $v_{ki}^{+/-}$, $k = 1, \dots, T_i$ yields either an *S-System* or a *General-Mass-Action (GMA)* system, respectively.¹ Consequently, the canonical BST formulation of an S-system with n dependent and m independent variables has the format [36]

$$\dot{X}_i = \alpha_i \prod_{j=1}^{n+m} X_j^{g^{ij}} - \beta_i \prod_{j=1}^{n+m} X_j^{h^{ij}}, \quad i = 1, \dots, n. \quad (3)$$

¹For the sake of completeness, a GMA system is given by

$$\dot{X}_i = \sum_{k=1}^{T_i} \pm \gamma_{ik} \prod_{j=1}^{n+m} X_j f^{ikj}, \quad i = 1, \dots, n$$

All positive (negative) terms in the above equation are aggregated into the first (second) term on the right hand side of (3). As the name implies, GMA systems are generalized mass action formulations and allow for non-integer valued kinetic orders. In that sense, allowing the kinetic orders to assume any real number renders a GMA model more flexible.

Rate terms of the form (2) are in general *approximations* to the real dynamics of the specific process. Consequently, the parameters $\Theta_S = \{g_{ij}, h_{ij}, \alpha_i, \beta_i\}, i = 1, \dots, n; j = 1, \dots, n + m$ of an S-system can be derived from the base system as [36]

$$g_{ij}, h_{ij} = \frac{\partial \log \left(\sum_{k=1}^{T_i} v_k^{+,-} \right)}{\partial \log X_j} \Bigg|_{\mathbf{X}=\mathbf{X}_0} = \frac{\partial \left(\sum_{k=1}^{T_i} v_k^{+,-} \right)}{\partial X_j} \Bigg|_{\mathbf{X}=\mathbf{X}_0} \frac{X_j}{\left(\sum_{k=1}^{T_i} v_k^{+,-} \right)}, \quad (4)$$

$$\alpha_i, \beta_i = v_i^{+,-}(\mathbf{X}_0) \prod_{j=1}^{n+m} X_j^{-g_{ij}, h_{ij}}. \quad (5)$$

In (4) and (5) $\mathbf{X}_0 = [X_{1_0}, \dots, X_{n_0}]^T$ is the *operating point* at which the S-system is constructed. At this operating point, equality holds between the base biochemical system and its corresponding S-system form.

We introduce S-systems here since, in Sec. VI, we make use of their convenient mathematical properties which facilitate analytic steady-state analysis. We briefly outline these mathematical properties in the following.

B. Steady-State Analysis

The canonical S-system form has convenient mathematical properties which allow for the direct analytic calculation of its steady-state solution in the log-space as [36]

$$\mathbf{y}_{\text{int}} = \mathbf{L}\mathbf{y}_{\text{ext}} + \underbrace{\mathbf{M}\mathbf{b}}_{\mathbf{m}} \quad (6)$$

where the matrix $\mathbf{L} \in \mathbb{R}^{n \times m}$ contains the *log-gains* which relate changes in logarithms of independent (external) variables in $\mathbf{y}_{\text{ext}} \in \mathbb{R}^{m \times 1}$ to changes in logarithm of dependent (internal) variables $\mathbf{y}_{\text{int}} \in \mathbb{R}^{n \times 1}$.

Entries of \mathbf{L} , \mathbf{M} and \mathbf{b} are composed of functions of the S-system parameters Θ_S and are thus functions of Θ_R , i.e., the parameters of the original RRE following (4) and (5). Eq. (6) implies that the independent variables in \mathbf{y}_{int} are *linear* functions of the independent variables in \mathbf{y}_{ext} with the slope of the resulting line given by the entries $l_{ij} = \frac{\partial X_i}{\partial X_j} \frac{X_j}{X_i}, i = 1, \dots, n; j = 1, \dots, m$ of \mathbf{L} and the constant offset given by element of the vector \mathbf{m} resulting from the matrix-vector product $\mathbf{M}\mathbf{b}$.

We use the form of (6) in the application to a bacterial sensor model in Sec. VI to directly obtain steady-state figures that can be linked to general sensors properties.

Considering the optimization and engineering of bacterial sensors as the main goal of this work, we then proceed with an analysis of how these sensor properties depend on the sensor model parameters. Formally, we achieve that through a *sensitivity analysis*.

C. Steady-State Sensitivities

From (6) one can directly obtain the sensitivities of the steady-state solutions \mathbf{y}_i with respect to the S-system parameters Θ_S and in extension of Θ_R . The *relative* sensitivities

$S_{l_{ij}, \theta_k}, S_{m_i, \theta_k}$ are calculated for $l_{ij} \in \mathbf{L}$ and $m_i \in \mathbf{m}$ using the chain-rule as [37]

$$S_{l_{ij}, \theta_k} = \frac{\partial l_{ij}}{\partial \theta_k} \left| \frac{\theta_k}{l_{ij}} \right| = \sum_{f \in \Theta_S} \frac{\partial l_{ij}}{\partial f} \frac{\partial f}{\partial \theta_k} \times \left| \frac{\theta_k}{l_{ij}} \right|, \quad (7)$$

$$S_{m_i, \theta_k} = \frac{\partial m_j}{\partial \theta_k} \left| \frac{\theta_k}{m_j} \right| = \sum_{f \in \Theta_S} \frac{\partial m_i}{\partial f} \frac{\partial f}{\partial \theta_k} \times \left| \frac{\theta_k}{m_i} \right|, \quad (8)$$

$$\theta_k \in \Theta_R, \tilde{\Theta}_S \subseteq \Theta_S, i = 1, \dots, n, j = 1, \dots, m.$$

Eqs. (7) and (8) evaluate the *percentage* changes in \mathbf{L} and \mathbf{m} due to infinitesimal percentage changes in $\theta_k \in \Theta_R$. We use these measures to investigate the contribution of biological parameters to the steady-state behavior of bacterial sensors.

D. Dynamics Sensitivities

In addition to the steady-state treatment, we conduct a *dynamic sensitivity analysis* for bacterial sensor models. Here we assume that the investigated biochemical system has *no* independent variables as the kinetics of the analyte state variable are now affected by the system dynamics.

With $\mathbf{f}_c \in \mathbb{R}^{n \times 1}$ comprising elements $\partial \dot{X}_i / \partial \theta_k, i = 1, \dots, n, \theta_k \in \Theta_R, \mathbf{J} \in \mathbb{R}^{n \times n}$ as the Jacobian with entries $\partial \dot{X}_i / \partial X_j, i, j = 1, \dots, n$ and dynamic sensitivity vector $\mathbf{z}_k \in \mathbb{R}^{n \times 1}$ with entries $\partial X_i / \partial \theta_k$ [38],

$$\dot{\mathbf{z}}_k = \mathbf{f}_c + \mathbf{J}\mathbf{z}_k, \quad k = 1, \dots, F \quad (9)$$

denote the differential equations of the dynamic sensitivities with respect to parameter θ_k . An ODE system consisting of ($F \cdot n$) equations of the form (9) can then be solved numerically to yield the final dynamic sensitivities \mathbf{z} that describe the temporal evolution of the sensitivities. This provides insight into how different phases of the time-course dynamics of a variable X_i responds to changes in parameters Θ_R .

One can further include the initial conditions of \mathbf{X} into Θ_R to investigate their effects on the system dynamics. In fact, by calculating the *relative dynamic sensitivity* with respect to the initial condition $X_j(0)$ of the *dependent* variable X_j , i.e.,

$$S_{i, X_j(0)} = \frac{\partial X_i}{\partial X_j(0)} \frac{X_j(0)}{X_i}, \quad i, j = 1, \dots, n \quad (10)$$

a measure is obtained which is very similar to the *dynamic log-gain* [39]. The dynamic log-gain can be used to evaluate the influence of changes in independent variables on the time-course of the investigated state-variable. Eq. (10), in contrast, assumes X_j to be dependent, hence the sensitivity with respect to its initial condition is measured.

We can then proceed to calculate the sensitivities of $S_{i, X_j(0)}$ with respect to other model parameters $\theta_k \in \Theta_R$ by solving the following differential equation (for derivation see Appendix B):

$$\begin{aligned} \frac{d}{dt} \left(\frac{\partial S_{i, X_j(0)}}{\partial \theta_k} \right) &= - \left(\frac{\partial S_{i, X_j(0)}}{\partial \theta_k} X_i + S_{i, X_j(0)} \frac{\partial X_i}{\partial \theta_k} \right) \frac{\dot{X}_i}{X_i^2} \\ &+ X_j(0) \frac{\partial X_i}{\partial X_j(0)} \left(2X_i^{-3} \dot{X}_i - X_i^{-2} \frac{\partial \dot{X}_i}{\partial \theta_k} \right). \end{aligned} \quad (11)$$

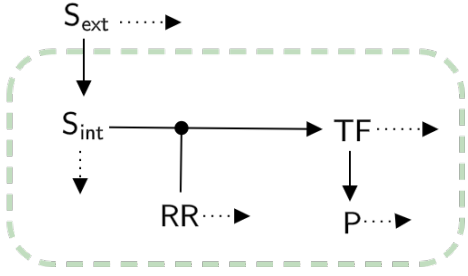


Figure 2. Structural diagram of a bacterial sensor. The dotted arrows indicate that all species are subject to degradation.

Eq. (11) constitutes the dynamic sensitivity analysis equivalent of (7). As it shares terms with (9), it can be integrated with \dot{z}_k into an extended ODE system.

IV. DISSECTING THE BACTERIAL SENSOR DETECTION CHAIN

The signal transduction pathway depicted in Fig. 2 shall serve as reference for the analysis of the various distinct steps in the detection chain of a bacterial sensor and the respective computational models. In the most general sense, the target analyte S_{ext} is *internalized* by a sensor cell and then potentially undergoes *modification* in interaction with response regulator RR. The resulting transcription factor TF subsequently drives the *expression* of the gene coding for the reporter protein P. Importantly, the internalization of the effector S_{ext} can either occur directly or indirectly by effect only. This is the case of the *phosphorylation* of an internal response regulator caused by an effector-bound cell surface receptor. We dissect the detection chain into its distinct processes and analyze their mathematical models. These models are initially provided as ordinary chemical reaction rate equations, since models of this form are most intuitive and generally a good starting point for a computational analysis. We note that parts of this section do not present new findings but collects information from various sources. We deem it necessary to proceed in this fashion as the presented information is crucial to comprehensively discussing bacterial sensor dynamics.

A. Internalization

The first step in the bacterial sensor detection chain is the uptake of the target analyte S_{ext} into the bacterial sensor cells (Fig. 2). The variety of bacteria strains exhibit a multitude of different uptake mechanisms that vary in their biochemical dynamics. The transport mechanisms can be categorized into the following groups:

Diffusion: In many bacteria nutrients or molecular signals *diffuse* into the bacterial cells across the cell wall. This is a passive process and requires no energy expenditure by the cell. This process can generally be described by Fick's law of diffusion across a membrane as [29], [40]

$$\frac{dS_{\text{int}}}{dt} = -q_D \left(\frac{S_{\text{int}}}{V_i} - \frac{S_{\text{ext}}}{V_e} \right) - \delta_s S_{\text{int}} \quad (12)$$

where S_{ext} and S_{int} denote the external and internal amount of target analyte, respectively, V_i and V_e are the intracellular and

extracellular volumes and δ_s is the degradation rate constant of S_{int} . The constant q_D collects the cell wall thickness, the diffusion coefficient and the cell membrane surface area. The expression in parentheses models the concentration gradient across the cell wall. If the external analyte amount S_{ext} is sufficiently high or subject to a constant supply, corresponding to *Scenario 1* described in Sec. V, it can be treated as constant \bar{S}_{ext} .

Considering that the uptake process is linear and time-invariant (LTI), it can thus be represented in form of an impulse response given by

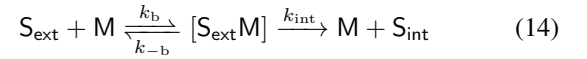
$$h_{\text{up}}(t) = \mathcal{F}^{-1} \left\{ \frac{\frac{q_D}{V_e}}{j\omega + \frac{q_D}{V_i} + \delta_s} \right\} = u(t) \frac{q_D}{V_e} e^{-\left(\frac{q_D}{V_i} + \delta_s\right)t} \quad (13)$$

where $u(t)$ is the unit step function and $\mathcal{F}^{-1}\{\cdot\}$ denotes the inverse Fourier transform.

Facilitated Diffusion and Active Transport Mechanisms:

In facilitated diffusion molecules are transported into the cell by means of membrane proteins or permeases. Facilitated diffusion is a passive process and is driven by a concentration gradient. Active transport mechanisms generally require an energy expenditure. As the number of transport proteins on the cell surface is finite, both processes are inherently saturable regardless of the external concentration which is the main difference to free diffusion.

With the signal or effector molecule S_{ext} and the surface permease M, the reaction equation for this process is given by



where k_b (k_{-b}) is the forward (backward) reaction rate constant of the binding reaction and k_{int} is the internalization rate constant.

Mathematically, the molecular uptake mechanisms follow saturation dynamics and can thus be described using Michaelis-Menten kinetics as

$$\frac{dS_{\text{int}}}{dt} = \kappa_{\text{up}} \left(\frac{S_{\text{ext}}}{K_{\text{up}} + S_{\text{ext}}} \right) \quad (15)$$

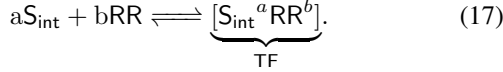
where the parameters κ_{up} and K_{up} are the maximum internalization rate and concentration at half maximum, respectively. They are explicitly derived from (14) as $\kappa_{\text{up}} = M_0 k_{\text{int}}$, where M_0 is the initial permease amount at $t = 0$ and $K_{\text{up}} = \frac{k_{-b} + k_{\text{int}}}{k_b}$, following Michaelis-Menten derivations. Similar modeling approaches have been discussed in the literature [41], [42]. For instance, in the literature K_{up} is occasionally used to characterize the kinetic uptake properties of a specific permease [43]. Eq. (15) is non-linear and it is thus not straightforward to derive a transfer function or impulse response for it. However, for relatively low concentrations $S_{\text{ext}} \ll K_{\text{up}}$, eq. (15) can be treated as linear which facilitates derivation of the corresponding LTI model which is given by

$$h_{\text{up}}(t) = u(t) \frac{\kappa_{\text{up}}}{K_{\text{up}}} e^{-\delta_s t}. \quad (16)$$

B. Transcription Factor Activation and Analyte Modification

Inside the bacterial sensor cell, the effector molecules either directly act as transcription factor TF for a specific gene or

undergo a series of reactions and interactions with regulatory proteins or response regulators RR, to form the TF complexes. This is described by the reaction equation



a and b denote the moieties of the species partaking in reaction (17). Depending on the precise reaction nature, the conceivable reaction dynamics range from linear (in case of a monomer transcription factor) to highly non-linear (for multimers). This is reflected by the reaction rate equations

$$\frac{d\text{TF}}{dt} = k_1 \left(\frac{S_{\text{int}}}{V_i} \right)^a \text{RR}^b - \delta_{\text{TF}} \text{TF} \quad (18)$$

with δ_{TF} denoting the degradation rate constant of TF. In (18), the division of S_{int} by the bacterial cell volume V_i is due to the units of the bi-molecular rate constant k_1 ($\mu\text{m}^3 \text{a} \text{min}^{-1}$) [31].

Due to the product of two state variables S_{int} and RR in (18), and the resulting non-linearity, the derivation of a system function or impulse response is challenging. With the assumptions of singular moieties on part of S_{int} , i.e., $a = 1$ and of abundance of response regulator with $\text{RR} \gg S_{\text{int}}$, it is, however, feasible. In this case RR^b can be treated as a constant parameter because the reaction with S_{int} does not substantially change the concentration of RR^b . Then, the impulse response can be given by

$$h_{\text{mod}}(t) = \mathcal{F}^{-1} \left\{ \frac{\frac{k_1}{V_i} \text{RR}^b}{j\omega + \delta_{\text{TF}}} \right\} = u(t) \frac{k_1}{V_i} \text{RR}^b e^{-\delta_{\text{TF}} t}. \quad (19)$$

In case of a multimerization with $a > 1$, the process is highly non-linear and an impulse response can only be derived by employing more elaborate techniques such as Volterra series analysis [8].

As stated above, a signal transduction pathway can comprise an indirect uptake mechanism where the analyte molecule is not entering the cell directly, but binds to a surface permease leading to the modification of the intracellular response regulator. This process is termed *phosphorylation*.

1) *Phosphorylation*: A common mechanism by which intracellular RR is turned on is *phosphorylation*. When the target analyte extracellularly binds to the receptor on the cell surface, a phosphate group is transferred from the intracellular surface receptor component to the free RR. For an arbitrary RR (with phosphorylated form RR_p which then acts as transcription factor) and a surface receptor C (with bound state C_b) this can be modeled as [31]

$$\frac{dC_b}{dt} = k_B \frac{S_{\text{ext}}}{V_e} C - k_{B-} C_b - \delta_{C_b} C_b \quad (20)$$

$$\frac{d\text{RR}_p}{dt} = k_p \text{RR} \frac{C_b}{V_i} - k_{p-} \text{RR}_p - \delta_{\text{RR}_p} \text{RR}_p. \quad (21)$$

k_B , k_{B-} , k_p and k_{p-} are the reaction rate constants for binding, unbinding, phosphorylation and dephosphorylation, respectively. We note that the total number of surface receptors in free or bound state is constant, i.e., $\tilde{c} = C + C_b$ following the *conservation of mass* rule. Under the condition that the phosphorylation of RR does not affect its stability ($\delta_{\text{RR}} = \delta_{\text{RR}_p}$),

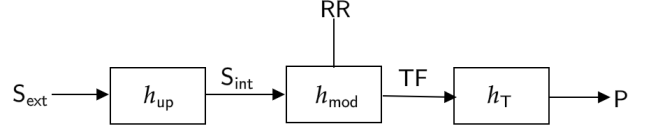


Figure 3. Block diagram of the LTI model of a bacterial sensor.

it also applies that $\widetilde{\text{RR}} = \text{RR} + \text{RR}_p$. From this follows that (20) and (21) can be written without explicit dependence on C and RR as

$$\frac{dC_b}{dt} = k_B \frac{S_{\text{ext}}}{V_e} (\tilde{c} - C_b) - k_{B-} C_b - \delta_{C_b} C_b \quad (22)$$

$$\frac{d\text{RR}_p}{dt} = k_p \frac{C_b}{V_i} (\widetilde{\text{RR}} - \text{RR}_p) - k_{p-} \text{RR}_p - \delta_{\text{RR}_p} \text{RR}_p. \quad (23)$$

C. Transcription and Translation

In the final step of the detection chain of a bacterial sensor, the TF complex binds to DNA segments known as promoter and thereby regulates gene expression. This regulation can manifest either as up-regulation (activation) or repression (inhibition; not treated here) of gene expression. The precise mechanism that underlies this essential process justifies closer inspection which is provided in Appendix Sec. A. This analysis finally yields the reaction rate equation for a reporter protein P as

$$\frac{dP}{dt} = \alpha_T \left[\kappa_B + \kappa_P \left(\frac{\text{TF}^{n_{\text{Hill}}}}{K^{n_{\text{Hill}}} + \text{TF}^{n_{\text{Hill}}}} \right) \right] - \delta_P P. \quad (24)$$

α_T denotes the translation efficiency, κ_B is the basal transcription rate, κ_P is the maximum up-regulated transcription rate, K is the Michaelis-Menten constant for transcription, n_{Hill} is the Hill coefficient and δ_P the decay rate constant of the reporter protein.

With $\text{TF} \ll K$, $n_{\text{Hill}} = 1$ and assuming no basal transcription ($\kappa_B = 0$), eq. (24) can be modeled as an LTI system, i.e.,

$$h_T(t) = u(t) \alpha_T \frac{\kappa_P}{K} e^{-\delta_P t}. \quad (25)$$

V. BACTERIAL SENSOR MODELS

With the mathematical descriptions for the single steps in the detection chain, it is now possible to construct full mathematical models of different bacterial sensor architectures. First, we outline under which conditions a bacterial sensor follows an LTI model. We then briefly discuss how the effects of bacterial population dynamics can be accounted for in a population-level bacterial sensor. Finally, we present a full bacterial sensor model of a real bacterial sensing system based on the strain *Streptococcus mutans*.

A. Linear Model for Bacterial Sensor

It is possible to construct a *linear* bacterial sensor model if the following conditions are met:

- Uptake via diffusion *or* active uptake modeled using Michaelis-Menten kinetics with analyte concentrations $S_{\text{ext}} \ll K_{\text{up}}$

- Analyte modification following (19) with analyte moiety of $a = 1$
- Transcription and translation following a Michaelis-Menten model with $n_{\text{Hill}} = 1$ with $\text{TF} \ll K$

The full detection chain of the sensor is then described by an LTI model visualized in Fig. 3 where each step in the detection chain, i.e., uptake, modification and transcription/translation is symbolized by a block representing the process's impulse response. The significance of this approach is that the output protein P can be expressed directly as

$$P(t) = \underbrace{h_{\text{up}}(t) * h_{\text{mod}}(t, \text{RR}) * h_{\text{T}}(t)}_{h_{\text{BS}}(t)} * S_{\text{ext}}(t) \quad (26)$$

where $*$ denotes convolution and $h_{\text{BS}}(t)$ the total impulse response of the bacterial sensor cell. In (26), the parametrization of $h_{\text{mod}}(t, \text{RR})$ by RR is made explicit to emphasize the condition under which (19) applies.

B. Whole Cell Bacterial Sensor - Population Dynamics

A population-level bacterial sensor harvests the bioluminescent response of an entire bacterial population; it is thus necessary to incorporate the population size into the model. Consequently, $\nu(t)$ models the size of the bacterial sensor strain at time t .

Bacterial populations undergo specific phases in the course of their growth cycle: the lag phase, the log-phase, the stationary phase and the death phase. Numerous mathematical models and iterations on the classical sigmoidal growth model for describing these dynamics have been published [44]. Our model is based on a variation of the original Verhulst growth model [45], where our contribution is the incorporation of a *delay* into the the governing differential equation.

The sensor strain's growth dynamics are then more accurately described by

$$\frac{d\nu}{dt} = \mu\nu(t) \left(1 - \frac{\nu(t - \tau)}{K_\nu} \right)^{b_\nu} \quad (27)$$

where μ denotes the population growth constant and the carrying capacity K_ν reflects the limits a bacterial population's growth is subjected to in a specific environment. b_ν is an additional scaling parameter that describes the populations capability to exceed the carrying capacity ($b_\nu > 1$) or to stay below it ($b_\nu < 1$). Eq. (27) is a delay-differential equation with delay τ and is chosen to capture an overshoot in the populations growth cycle where its size initially exceeds the systems carrying capacity and subsequently levels off. We chose this modeling approach to explain our experimental data obtained from wet-lab experiments (Fig. 4).

C. *Streptococcus mutans* as Sensor for XIP

For the bacterial sensor investigated in this paper, we choose the bacterium *Streptococcus mutans* (*S. mutans*). This Gram-positive bacterial strain is found in the human oral cavity and is the primary cause for tooth decay [46]. In *S. mutans*, natural competence, i.e., the ability of bacteria to take up naked DNA from their environment and incorporate it into

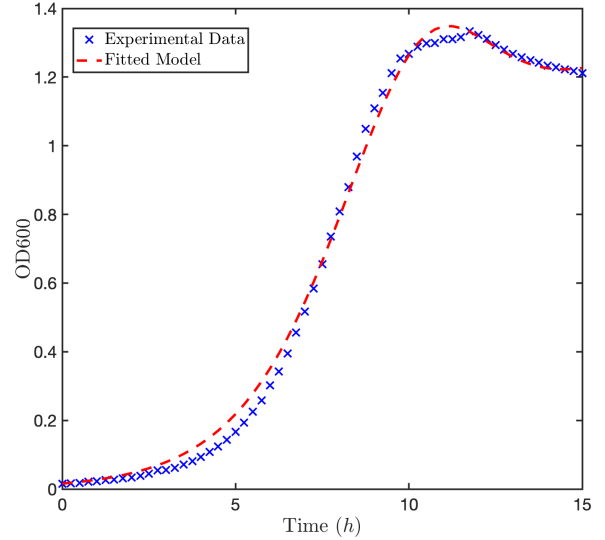


Figure 4. Experimental bacterial optical density (OD600) for *Streptococcus mutans* vs. delay-differential equation model with fitted parameters $K_\nu = 7.5603 \times 10^8$, $\mu = 0.0090224 \text{ min}^{-1}$, $\tau = 80.5438 \text{ min}$ and $b_\nu = 1$.

their genomes as survival- and adaption strategy, is regulated by pheromones/peptides [47]. *S. mutans* exhibits two signaling pathways over which two distinct peptides function as signals: the CSP and the XIP pathway. Both pathways activate the promoter of *sigX*, the master regulator of competence.

In this paper, we focus on the distinct XIP signaling pathway. Extracellular XIP (SigX-inducing peptide) is imported by the cell-membrane bound oligopeptide permease (OPP). The imported XIP activates the free form of the intracellular response regulator (ComR_f) by building a dimer (i.e., involving two molecules of XIP and free ComR each) ComR_m which, in turn, activates the transcription of *sigX*. Recent studies suggest that ComR_m further acts as transcription factor for *comR* [48] which implies a positive feedback loop in the XIP signaling pathway (Fig. 5). In a wild-type *S. mutans* strain, ComR_m further acts as a transcription factor for *comS* which codes for the intracellular XIP-precursor ComS. Since *S. mutans* produces and secretes XIP (or ComS) naturally, we knock out the *comS* gene in the *S. mutans* sensor strain to ensure that no endogenous XIP is produced thereby eliminating this source of 'noise'.

For this experiment we use the *lucFF* gene as a reporter system. To construct the reporter system, first the *sigX* promoter region is amplified and cloned upstream of the *luc* gene. Both genes are consequently expressed at the same rate when activated by the mature transcription factor (Fig. 5).

Complying with the steps in the detection chain of *S. mutans*, we formulate (29)-(34) as a computational model for the *S. mutans*-XIP bacterial sensor. Eqs. (29) and (30) model the time evolution of the intracellular XIP amount and extracellular XIP amount, respectively. The uptake mechanism is modeled using an active uptake model. Eq. (31) captures the kinetics of the intracellular ComR_f regulator which is transcribed at a basal rate κ_B . ComR_f's rate of production is

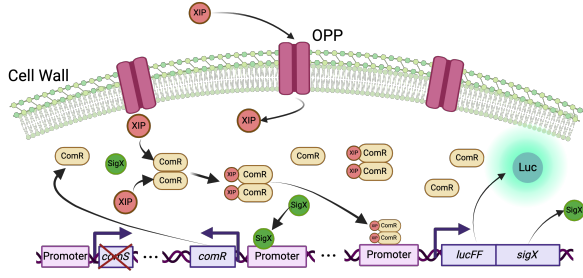


Figure 5. Transcriptional activation of *sigX/lucFF* operon in engineered *S. mutans* strain. (Illustration was created with BioRender.com).

further up-regulated by the master transcription factor SigX which is reflected by the Michaelis-Menten term in (31) [48]. As stated above, the immature ComR_f is activated by intracellular XIP_{int} with which it forms a dimer which is the mature form of ComR_f (ComR_m) that acts as TF for *sigX*. The study on the ComRS pathway in *Streptococcus thermophilus* [32] suggests that the stoichiometry of the dimerization is such that *two* ComR and *two* XIP molecules are needed to produce *one* mature ComR_m molecule. This is reflected by the exponent 2^2 in (29), (31) and (32), and the factor 2 in (29) and (31). Eqs. (33) and (34) model the gene transcription and subsequent translation (reflected by the translation efficient parameter α_{sigX}) of mRNA into the respective proteins, luciferase and SigX. The identical terms in both equations reflect that luciferase and SigX are produced at *identical rate*. The gene expression of both genes *sigX* and *lucFF* is activated by the transcription factor ComR_m and the corresponding transcription rate is governed by Michaelis-Menten kinetics.

As stated, the total bioluminescence response L_B of the sensor population is directly proportional to the amount of luciferase in the system and is thus commonly modeled as

$$L_B = \xi_{\text{lum}} \text{Luc} \quad (28)$$

where ξ_{lum} is a proportionality constant which collects the effects of, for example, oxygen availability, substrate concentration, etc. The model is highly simplifying and a more precise model (e.g., [49]) would additionally consider residual substrates which participate in the bioluminescence reaction.

1) *Parameter Estimation*: We proceed to fit the computational *S. mutans* model to experimentally obtained data by adjusting the equation system's parameters. We consider the *average response* of a bacterial cell which is given by (29)–34 *discounting* the scaling effect of the bacterial population factor $\nu(t)$. We use our wet-lab data of the form $\text{RLU}/\text{OD600}$, i.e., luminescence data in Relative-Light-Units (RLU) normalized with measured OD600 population density curves (see Fig. 4). The resulting data can be taken as measure of the average response of a viable bacterial cell in the population.

As we do not know ξ_{lum} , estimating the parameters of the model from the experimental data is greatly complicated. We note that ξ_{lum} could experimentally be obtained by calibrating

²It must be noted that, in general, this exponent can also assume values different to the moieties of the reactants.

the luminescence reader through parallel measurements of the luciferase protein (e.g., western blotting) and comparison with the obtained RLU curves. Here, we proceed by assuming a value $\xi_{\text{lum}} = 10^4$ which is sensible in the context of reasonable estimation ranges for the model parameters. We further possess only limited observations of the system (in form of the measured luminescence as proxy for the luciferase concentration), lacking data for the intermediary species and processes. This, too, complicates estimating the full system parameters as they cannot be verified against data observed for the reactions they are *directly* linked to.

For the estimation, we restricted the optimization domain of parameters to biologically sensible ranges. For several parameters we relied on references in the literature as a guide for defining the estimation ranges or to fix the parameter values in the estimation process [32].

The results of the parameter adjustment is presented in Fig. 6 and Tab. I. The bacterial sensor system has been implemented for simulation and parameter estimation in *CO-PASI* [50]. The parameter estimation was conducted using a *Simulated Annealing* algorithm with a start temperature of $T = 1$ and a default cooling factor of 0.85. For our simulation and estimation we assumed a bacterial volume of $V_i = 1 \mu\text{m}^3$ and an *effective* extracellular volume of $V_e = 10 \mu\text{m}^3$ per cell.

2) *Experimental procedure*: The experimental wet-lab data was obtained as follows:

a) *Bacterial strains and medium*: Cultures of *S. mutans* (strain SM091 [51]) were grown in chemically defined medium (CDM) at 5% CO_2 , 37 °C and stored at –80 °C in the same medium supplemented with 15% glycerol for cryopreservation. CDM is prepared as previously described [52].

b) *Synthetic peptide*: The *sigX*-inducing peptide (XIP) ($\text{NH}_2\text{-GLDWWSL-COOH}$; 98% purity; GenScript, Piscataway, NJ, USA) was reconstituted with 20 μL dimethyl sulfoxide (DMSO) (Sigma-Aldrich, St. Louis, MI, USA), to which 1 mL sterile distilled water was added to give a final concentration of 10 mM and stored at –20 °C. Working stocks were prepared and aliquoted at 100 μM in sterile distilled water and stored at –20 °C.

c) *Luciferase reporter assays*: Culture stock of *S. mutans* reporter strain at OD600 of 0.5 was thawed and diluted 5-fold in CDM. Serial dilutions of XIP were made (2000 nM, 1000 nM, 500 nM, 250 nM, 125 nM, 62.5 nM, 31.25 nM, 15.625 nM, 7.8 nM, 3.9 nM, 1.9 nM and control (No XIP added) in 200 μL of CDM aliquoted in wells of a 96-well microtiter plate (Thermo Fisher Scientific). Then, 100 μL of previously diluted *S. mutans* culture was added to the wells, in triplicates for each XIP concentration. A volume of 10 μL of a 1 mM aqueous D-luciferin solution (Synchem, Felsberg-Altenberg, Germany) was added to each well, and three wells containing CDM and luciferin without the inoculum were used as blanks. The plate was sealed with a Top Seal (PerkinElmer), and incubated at 37 °C for 15 hours. Relative luminescence units (RLU) and OD600 were measured every 15 minutes in a multi-detection micro plate reader (Cytation 3; BioTek).

$$\begin{aligned} \frac{dXIP_{\text{int}}}{dt} &= \nu(t)\kappa_{\text{up}} \left(\frac{XIP_{\text{ext}}}{K_{\text{up}} + XIP_{\text{ext}}} \right) - \delta_{X_{\text{int}}} XIP_{\text{int}} \\ &\quad - 2k_{\text{TF}_m} \left(\frac{1}{\nu(t)V_i} XIP_{\text{int}} \text{ComR}_f \right)^2 + 2k_{\text{TF}_f} \text{ComR}_m \end{aligned} \quad (29)$$

$$\frac{dXIP_{\text{ext}}}{dt} = -\nu(t)\kappa_{\text{up}} \left(\frac{XIP_{\text{ext}}}{K_{\text{up}} + XIP_{\text{ext}}} \right) - \delta_{X_{\text{ext}}} XIP_{\text{ext}} \quad (30)$$

$$\begin{aligned} \frac{d\text{ComR}_f}{dt} &= \nu(t)\alpha_{\text{ComR}}\kappa_B - \delta_{\text{TF}_f} \text{ComR}_f - 2k_{\text{TF}_m} \left(\frac{1}{\nu(t)V_i} XIP_{\text{int}} \text{ComR}_f \right)^2 \\ &\quad + 2k_{\text{TF}_f} \text{ComR}_m + \nu(t)\alpha_{\text{comR}}\kappa_x \left(\frac{\left(\frac{\text{SigX}}{\nu(t)V_i} \right)^m}{K_{\text{SigX}}^m + \left(\frac{\text{SigX}}{\nu(t)V_i} \right)^m} \right) \end{aligned} \quad (31)$$

$$\begin{aligned} \frac{d\text{ComR}_m}{dt} &= k_{\text{TF}_m} \left(\frac{1}{\nu(t)V_i} XIP_{\text{int}} \text{ComR}_f \right)^2 \\ &\quad - k_{\text{TF}_f} \text{ComR}_m - \delta_{\text{TF}_m} \text{ComR}_m \end{aligned} \quad (32)$$

$$\frac{d\text{Luc}}{dt} = \nu(t)\alpha_{\text{sigX}}\kappa_{\text{comR}} \left(\frac{\left(\frac{\text{ComR}_m}{\nu(t)V_i} \right)^n}{K_{\text{comR}}^n + \left(\frac{\text{ComR}_m}{\nu(t)V_i} \right)^n} \right) - \delta_L \text{Luc} \quad (33)$$

$$\frac{d\text{SigX}}{dt} = \nu(t)\alpha_{\text{sigX}}\kappa_{\text{comR}} \left(\frac{\left(\frac{\text{ComR}_m}{\nu(t)V_i} \right)^n}{K_{\text{comR}}^n + \left(\frac{\text{ComR}_m}{\nu(t)V_i} \right)^n} \right) - \delta_x \text{SigX} \quad (34)$$

Table I
S. mutans-XIP SYSTEM PARAMETERS WITH ADJUSTED VALUES.

Parameter	Unit	Value	Description	Parameter	Unit	Value	Description
$\text{ComR}_f(0)$	-	17.25	Initial Response Regulator Amount	κ_B	min^{-1}	0.492	Basal comR Transcription Rate
κ_{up}	min^{-1}	18.35	Maximal Uptake Rate	κ_{ComR}	min^{-1}	6.63	Maximum ComR-induced sigX Transcription Rate
K_{up}	μm^{-3}	333.6	Michaelis-Menten Constant for Active Uptake	K_{ComR}	μm^{-3}	14.02	comR Michaelis-Menten Constant
δ_{XIP}	min^{-1}	0.023	Degradation Constant of XIP	α_{SigX}	-	2	sigX Translation Efficiency
k_{TF_m}	$\mu\text{m}^9 \text{min}^{-1}$	0.02	Transcription Factor Maturation Reaction Rate Constant	κ_X	min^{-1}	0.216	Maximum SigX induced comR Transcription Rate
δ_{TF}	min^{-1}	0.01	Degradation Constant of ComR (fixed) [32]	K_{SigX}	μm^{-3}	617413	sigX Michaelis-Menten Constant
k_{TF_f}	min^{-1}	0.00001	Transcription Factor De-Maturation Reaction Rate Constant	δ_x	min^{-1}	0.59	SigX Degradation Constant
δ_{TF_m}	min^{-1}	0.0027	Degradation Constant of ComR-XIP Complex	δ_L	min^{-1}	0.0158	Luciferase Degradation Constant (fixed) [32]
α_{ComR}	-	0.166	comR Translation Efficiency	n	-	2.81	Hill Coefficient
m	-	3.96	Hill Coefficient				

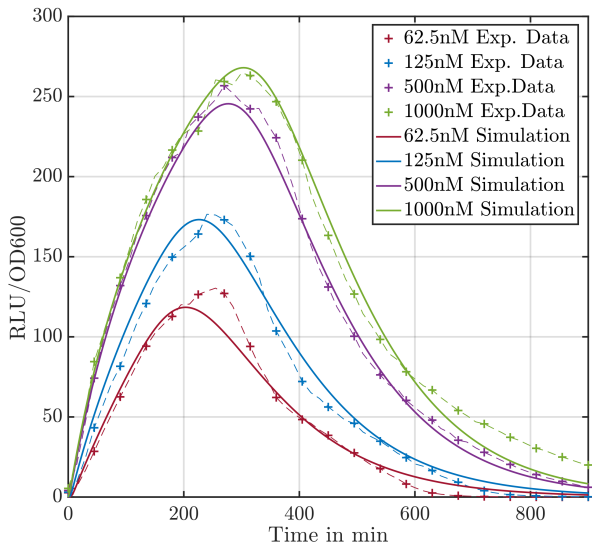


Figure 6. Experimental data vs. simulation of bacterial sensor luminescence response with fitted parameters. Experimental data is RLU data normalized with experimental OD600 bacterial growth curves.

VI. ENGINEERING AND OPTIMIZATION OF BACTERIAL SENSORS

While the focus so far was on the *description* of a generic bacterial sensor, we now proceed to investigate strategies for altering and engineering a bacterial sensor with specific properties. It is consequently useful to consider general aspects of sensor analysis and engineering. Important sensor properties are

- **Sensor sensitivity:** Differential response of the sensor to different measurand quantities, i.e., the difference between sensor outputs in response to different analyte concentrations.
- **Response intensity:** Generally, a stronger response of the bacterial sensor is clearly desirable for the maximization of the Signal-to-Noise-Ratio (SNR).
- **Responsiveness:** Time between first contact with analyte and *final* sensor response, i.e., discounting contingent overshoots during the transient response.³

In the following, we discuss how these general sensor properties (sensor sensitivity and response intensity) can be evaluated in the context of the investigated bacterial sensor models. As we aim at exploring how bacterial sensors can be *practically* altered and engineered for specific purposes, it is necessary to establish a link between *parameters* in our computational models and *biological properties* that are accessible to manipulation in the wet-lab.

A. Engineering of Bacteria - Linking Model Parameters to Biological Properties

Synthetic biology is devising ever more techniques for altering bacterial dynamics for specific purposes, e.g., genetic

³This is listed here for the sake of completeness but a formal treatment of this sensor property is not within the scope of this work.

or metabolic engineering. For this paper, we are most interested in strategies that can directly change a bacterial cell's properties that relate to the detection chain discussed above. We therefore briefly review a number of techniques by which bacteria can be manipulated to evoke desired sensor dynamics. Here, we merely give a qualitative overview. In each specific case, a quantitative relationship between a concrete manipulation measure and the exact change in model parameter must be established which is not within the scope of this work.

Regulation of Uptake: Active uptake mechanisms or phosphorylation-based internalization are governed by cell membrane-bound ligands or channel molecules. By regulating the expression of the genes coding for the specific permease protein one has control of the uptake dynamics of a sensor. Considering the *S. mutans*-XIP sensor, by *up-regulating* the expression of the *opp* gene we could *increase* the uptake rate constant κ_{up} due to its parametrization by M_0 which we introduced as the number of surface permeases per cell above.

Regulation of Protein Stability: The half-life of proteins involved in a biochemical system has a strong impact on its overall dynamics. The degradation rates of proteins in bacterial cell depend on a variety of factors: environmental conditions (e.g., pH, temperature), the proteins structure and concentration, or post-transcriptional modification (e.g., phosphorylation, bacterial ubiquitination). Techniques based on attaching *degradation tags* to proteins that mark them for degradation by the cellular protein regulation mechanisms [53] enhance the possibilities for engineering protein concentration level in a targeted manner. Degradation tags can thus be used to directly alter the protein degradation rate constants (see e.g., δ_L in (33)).

Regulation of Gene Expression: Engineering of gene expression is the single most important tool in synthetic biology. This comprises promoter engineering, plasmids which can be engineered for specific purposes and inserted into bacteria, and the targeted knocking out (see *comS* in *S. mutans*-XIP model above) or insertion of genes (e.g., promoter genes) directly into the bacterial genome. The number of plasmids inserted into bacterial cells, for example, directly modulates the expression levels of the genes on the plasmid as more promoter sites are available for binding transcription factors. According to Appendix Sec. A, the number of promoter sites thus directly modulates the transcription rate (e.g., κ_{comR} in (33)). Considering the *S. mutans*-XIP sensor example discussed above, this can be used to regulate transcription of the *sigX-lucFF* operon, or to control κ_B , i.e., the basal transcription rate of the response regulator. This facilitates a finer regulation of the modulation effect of the response regulator.

B. Steady-State Optimization

Using the introduced S-system formalism, we construct the S-system representation based on a RRE model of a generic bacterial sensor following the same structure as the discussed *S. mutans*-XIP model and investigate it with respect to the sensor properties listed above. This section treats the abundant-analyte case (corresponding to *Scenario 1* introduced in Sec. II). The parameter values of the RRE model used in

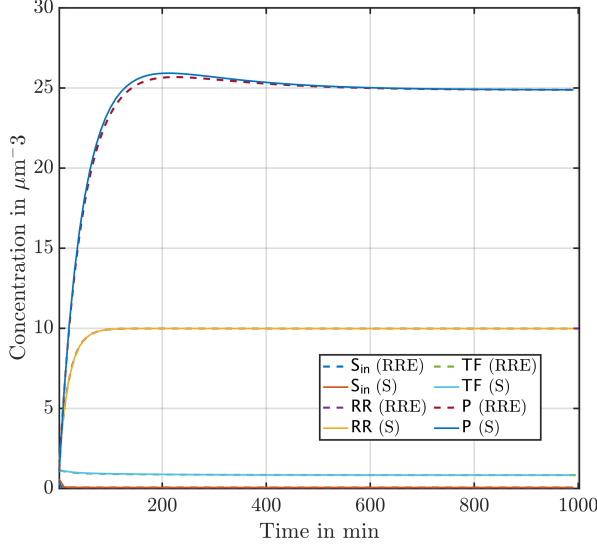


Figure 7. RRE- & S-system model numerical solution comparison.

this section are chosen somewhat arbitrary without reference to an actual bacterial sensor but we assumed realistic values for each parameter. For the transcription factor maturation reaction we assumed moieties of 1 for both reactants but allowed for non-unity reaction orders N and M .

RRE Model:

$$\begin{aligned} \frac{d}{dt} S_{in} = & \kappa_{up} \left(\frac{S_{ext}}{K_{up} + S_{ext}} \right) + k_{TF_f} TF \\ & - k_{TF_m} RR^M S_{in}^N - \delta_S S_{in} \end{aligned} \quad (35)$$

$$\begin{aligned} \frac{d}{dt} RR = & \underbrace{\alpha_{RR} \kappa_{RR}}_{\text{Basal Transcription}} + k_{TF_f} TF \\ & - k_{TF_m} RR^M S_{in}^N - \delta_{RR} RR \end{aligned} \quad (36)$$

$$\begin{aligned} \frac{d}{dt} TF = & k_{TF_m} RR^M S_{in}^N \\ & - k_{TF_f} TF - \delta_{TF} TF \end{aligned} \quad (37)$$

$$\frac{d}{dt} P = \frac{\alpha \kappa_{max} TF^{n_{Hill}}}{K^{n_{Hill}} + TF^{n_{Hill}}} - \delta_P P \quad (38)$$

S-System Model:

$$\begin{aligned} \frac{d}{dt} S_{in,S} = & \alpha_S TF_S^{g_{S,TF}} S_{ext,S}^{g_{ext,S}} \\ & - \beta_S RR_S^{h_{S,RR}} S_{in,S}^{h_{in,S}} \end{aligned} \quad (39)$$

$$\begin{aligned} \frac{d}{dt} RR_S = & \alpha_{RR} TF_S^{g_{RR,TF}} \\ & - \beta_{RR} RR_S^{h_{RR,RR}} S_{in,S}^{h_{in,S}} \end{aligned} \quad (40)$$

$$\begin{aligned} \frac{d}{dt} TF_S = & \alpha_{TF} RR_S^{g_{TF,RR}} S_{in,S}^{g_{in,S}} \\ & - \beta_{TF} TF_S^{h_{TF,TF}} \end{aligned} \quad (41)$$

$$\begin{aligned} \frac{d}{dt} P_S = & \alpha_P RR_S^{g_{P,RR}} TF_S^{g_{P,TF}} \\ & - \beta_P P_S^{h_{P,P}} \end{aligned} \quad (42)$$

Eqs. (35)-(38) are the RRE model of the bacterial sensor and (39)-(42) represent the corresponding S-system derived according to (4) and (5). The operating points of the S-system representation $\mathbf{X}_0 = [S_{in,0}, RR_0, TF_0, P_0]^T$ are chosen so that the steady-state solutions of both systems are near identical. The natural choice of \mathbf{X}_0 are the *steady-state solutions* of the RRE system. Solving the equation systems numerically yields solution trajectories as plotted in Fig. 7. Note that the transient responses of the S- and RRE-system representations can diverge significantly while the steady-state solutions are in general identical.

The S-system representation can then be analytically solved for steady-state as in (6) and the log-gain matrix \mathbf{L} obtained explicitly. Solving repeatedly for the steady-state bacterial sensor output P_{SS} with different values of the external/independent variable S_{ext} and plotting in the log-log space yields a line whose slope reflects the log gain of the sensor (Fig. 8a). The S-system used to generate the data is constructed around the numerically obtained RRE-system steady state solution for the mid-value of the tested external variable S_{ext} range. This reflects that a single S-system representation can accurately capture the system dynamics responding to a wider range of input values.

Next, the log-gain sensitivities S_{L_P, θ_k} and sensitivities S_{m_P, θ_k} are obtained using (7) and (8) to measure the relative change in the log-gain and the constant component of the steady-state sensor response in reaction to a relative change in a RRE model parameter θ_k . Importantly, and considering the above mentioned sensor properties, S_{L_j, θ_k} and S_{m_j, θ_k} constitute measures for *sensor sensitivity* and *response intensity*, respectively. The results of this sensitivity analysis are shown in Fig. 8b.

Noticeably, we find that S_{L_P, θ_k} and S_{m_P, θ_k} have opposite signs for a number of evaluated RRE parameters. This suggests that changes in several RRE system parameters have *diametric* effects on *sensor sensitivity* and *response intensity*. In other words, according to this analysis *increasing* the steady-state response strength of a bacterial sensor by manipulating a manipulable subset of these parameters (via techniques alluded to above) *diminishes* its sensitivity and vice versa.

C. Dynamic Sensitivity Analysis

While the preceding section investigates the *steady-state* response of a bacterial sensor, we now examine the case when the signal analyte is scarce (i.e., non constant; see *Scenario 2* described in Sec. II) and either is depleted naturally or enters the bacterial sensor system dynamics as a state variable without a compensating influx. We are interested in how the findings from the steady-state analysis map onto the time-course analysis of the sensor response.

For the dynamic sensitivity analysis, S_{ext} cannot be treated as external variable and enters the equation system (35)-38 as additional equation as (see also (30))

$$\frac{d}{dt} S_{ext} = -\kappa_{up} \left(\frac{S_{ext}}{K_{up} + S_{ext}} \right) - \delta_S S_{ext}. \quad (43)$$

Here we work with the RRE system directly as our focus is on the transient response. In particular, we isolate the

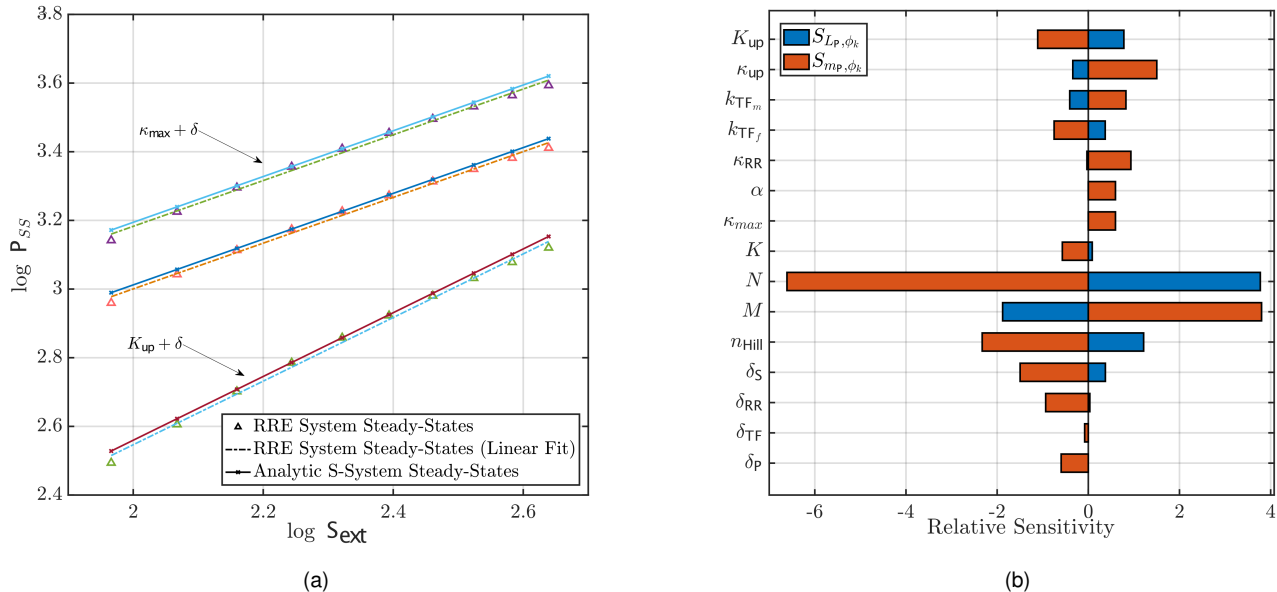


Figure 8. S-system steady-state sensitivity analysis. **(a)** Effect of parameter alterations on S-system steady-state solutions. The center graph group represents the base system with the initial parameter set. **(b)** Sensitivities with respect to model parameters.

maximum response as the point of interest as is common in the related literature. As above, we investigate the influence of model parameters on both sensor sensitivity and sensor signal intensity.

Response intensity is investigated by appending one set of differential equations (9) per investigated parameter to the ODE system (35)-38 and solving the resulting system numerically with an appropriate solver (we use the ODE15S solver in MATLAB). Thereby, trajectories as in Fig. 9a are obtained which are then sampled corresponding to the point of maximum transient response of the sensor output P, i.e., in the time-course solution of the sensor response, the time of maximum response $\tau_{\max P}$ is extracted and $S_{P,\theta_k}(\tau_{\max P})$ evaluated.

The entire dynamic sensitivity trajectory of the variable of interest with respect to a specific parameter predicts how a change in the parameter affects the time-course of the variable. For instance, the dynamic sensitivity for the parameter n_{Hill} predicts well how changes in it affect P (Fig. 9b).

As described in Sec. III-D, we can compute the dynamic sensitivity with respect to the amount of a species (state-variable) at $t = 0$ (i.e., the initial conditions of the corresponding ODE system). Doing so for P with respect to $S_{\text{ext}}(0)$, i.e., calculating $S_{P,S_{\text{ext}}(0)} = \frac{\partial P}{\partial S_{\text{ext}}(0)}$, yields the results shown in Fig. 10 where the sampled value, i.e., $S_{P,S_{\text{ext}}(0)}(\tau_{\max P})$, corresponds well to the slope of the line in the inset plot. The latter shows the maximum response of P evaluated for several values of $S_{\text{ext}}(0)$ in log-log space.

Equivalent to the steady-state log-gain sensitivities, we then proceed to investigate the impact of model parameters on $S_{P,S_{\text{ext}}(0)}$ by solving (11) for all $\theta_k \in \Theta_R$. The corresponding results are presented in Fig. 11.

Comparing Fig. 8b and Fig. 11b reveals that the sensitivities for steady-state and transient maximum exhibit notable differ-

ences. While, for instance, evaluating $S_{L_P,\kappa_{RR}}, \frac{\partial S_{P,S_{\text{ext}}(0)}}{\partial \kappa_{RR}}$ and $S_{P,\kappa_{RR}}$ implies that a positive change in κ_{RR} has only a minor effect on the steady-state log-gain (namely *decreasing* it), the maximum transient response experiences both a positive shift in magnitude *and* a minor increase in sensitivity (as is also visualized in Fig. 11a). Other trends observed in the steady-state analysis are, in contrast, reproduced by the dynamic sensitivity analysis; alterations in n_{Hill} , for example, elicit strong diametric effects on signal intensity and sensitivity for both cases.

The sensitivity analysis results for both steady-state and transient response presented in this section have validity in this form only for the arbitrary parameter set alluded to above. However, the general findings of the investigation could be confirmed for various tested parameter sets.

VII. CONCLUSION

In this work we systematically investigated the quantitative properties of the biochemical mechanisms governing bacterial sensor systems. We dissected the bacterial sensor detection chain and provided an overview of models for describing them. Based on this, we presented a *S. mutans*-XIP sensor as a case-example for which we fitted the derived model to experimental wet-lab data. We obtained a good match between our computational model and our empirical data yielding biologically meaningful parameter values which are in the expected ranges. While no general validity of the fitted parameter values can be guaranteed, the results demonstrate the applicability of the methodological approach. Our mathematical modeling approach is limited to deterministic models, which is adequate for the scope of this paper, but may be insufficient to study the inherent stochasticity of molecular systems in greater detail. Further, we applied rather

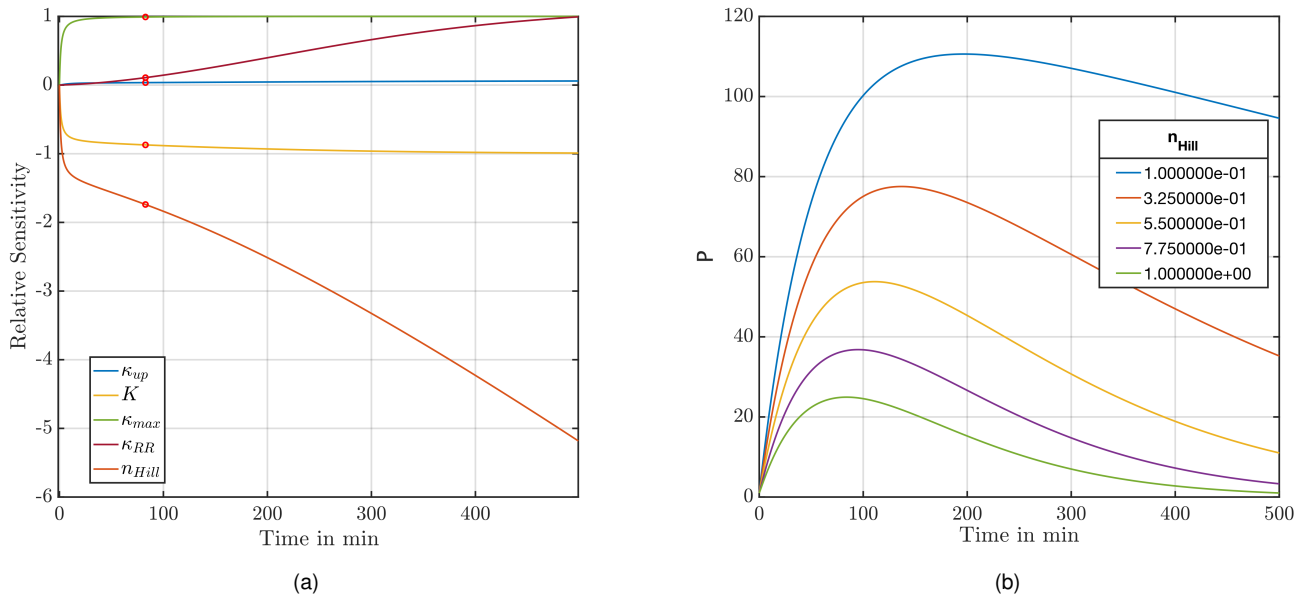


Figure 9. Dynamic Sensitivity Analysis. (a) Relative Dynamic Time-Course Sensitivities. Red circles mark evaluation at maximum response of P. (b) Sensor response over range of values of n_{Hill} .

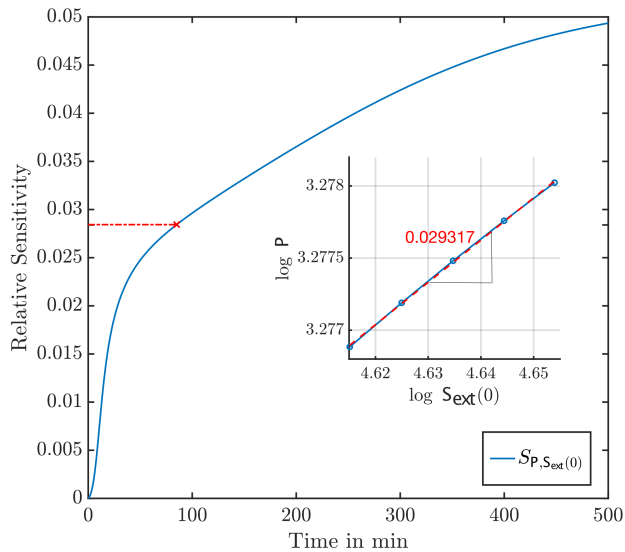


Figure 10. Dynamic Sensitivity with respect to $S_{ext}(0)$.

restrictive assumptions (aqueous assays, homogeneous analyte distribution, homogeneous expression levels of bacterial sensor cells) to the analysis. These shortcomings may be addressed in future works.

The main contribution of this paper is the analytic and numerical derivation of common sensor-engineering measures, e.g., the *sensor sensitivity*, for bacterial sensors systems. This was achieved by rigorous application of BST methods which yielded analytic results for the steady-state treatment of bacterial sensors. We compared these findings with results obtained from a dynamic time-course analysis where we focused on

the maximum response of a bacterial sensor. Specifically, we mathematically investigated how various parameters from the computational models influence log-gain (sensor sensitivity) and response strength levels for both steady-state and maximum sensor response. We found that, in many cases, with notable exceptions, parameter changes have opposite effects on bacterial sensor sensitivity and response intensity levels for both steady-state and maximum transient response. This implies a trade-off which must be taken into account when designing bacterial sensor systems. We mentioned the *responsiveness* of a sensor as crucial property but did not further investigate it in this work; this might be addressed in a future study.

We further identified and discussed a selection of parameters that are most accessible for manipulation from a bio-engineering perspective. A systematic investigation that links concrete manipulations in the wet-lab to numerical changes in model parameters may be considered for future research.

By combining biological expertise with multifaceted computational techniques, we aimed for complementing research in MC with a focus on the quantitative aspects of engineering and optimizing bacterial sensing systems. We expect that this work will contribute to guiding cross-disciplinary researchers who want to computationally investigate bacterial sensors.

APPENDIX A MODELING GENE TRANSCRIPTION

For the sake of completeness, the dynamics of gene expression in a bacterial sensor are summarized and a well-established mathematical representation is derived (see e.g., [12], [28]):

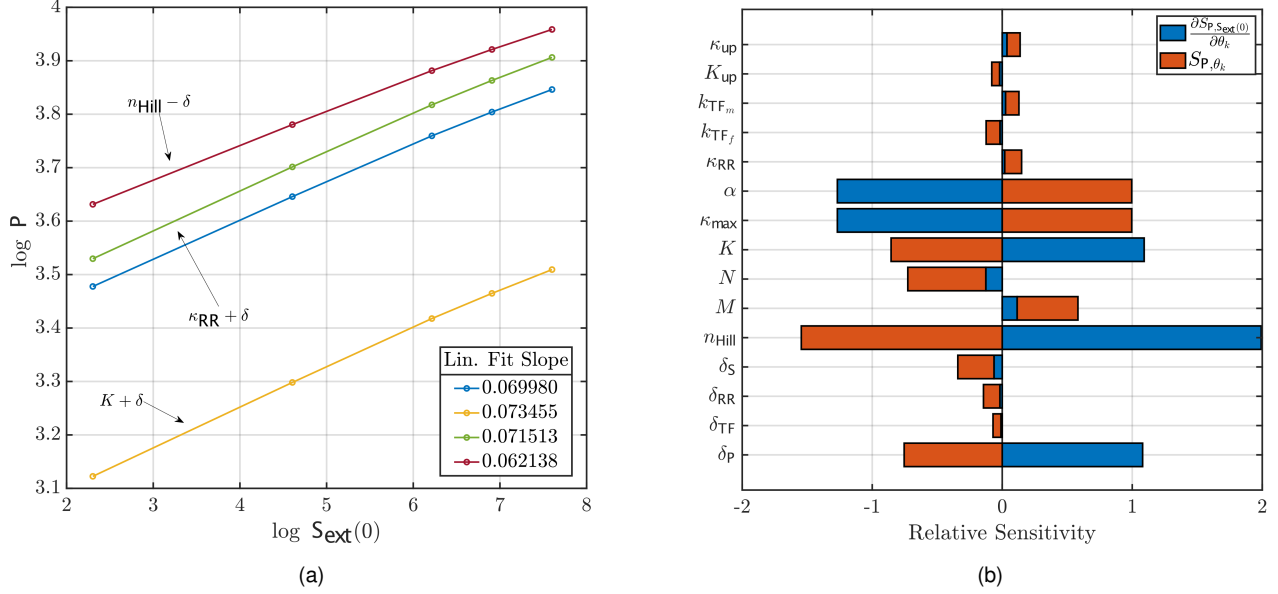


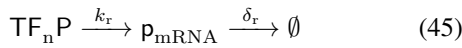
Figure 11. Dynamic Sensitivity Analysis Results. (a) Effect of parameter alterations. The blue line represents the base system with unaltered parameters. (b) Sensitivities for model parameters.

- Transcription factor TF binding to promoter Pr of a gene is reflected by the reaction equation



where k_a and k_d denote the forward and backward reaction rate constants. Here, n defines the affinity of the binding process and denotes the number of transcription factor molecules binding to a promoter site, thereby activating it and increasing its affinity for binding polymerase and thus initiating transcription.

- Transcription of a gene into mRNA p_{mRNA} follows the reaction equation



with transcription reaction rate constant k_T and decay rate constant δ_T .

- Translation of mRNA into protein P with rate constant k_T is reflected by



It is practical to exploit the different time-scales of promoter-TF binding and transcription, and the constant number of promoter sites to derive a compact expression for the process. Consequently, the transcription dynamics are conveniently described by Michaelis-Menten or Hill kinetics where the former is a special case of the latter and assumes a Hill coefficient of $n_{\text{Hill}} = 1$. n_{Hill} conceptually corresponds to the parameter in (44) where n_{Hill} can assume non-integer values. Consequently, transcription can be modeled as,

$$\frac{dp_{\text{mRNA}}}{dt} = \kappa_T \left(\frac{\text{TF}^{n_{\text{Hill}}}}{K^{n_{\text{Hill}}} + \text{TF}^{n_{\text{Hill}}}} \right) - \delta_T p_{\text{mRNA}} \quad (47)$$

with $K = \frac{k_d + k_T}{k_a}$ and $\kappa_T = \text{Pr}_0 k_T$.

The mRNA is then translated into protein with translation rate constant k_l following

$$\frac{dP}{dt} = k_l p_{\text{mRNA}} - \delta_P P. \quad (48)$$

With the quasi-steady-state assumption for p_{mRNA} (based on mRNA being in general much shorter lived relative to the corresponding protein which allows for the quasi-steady-state assumption for p_{mRNA}), solving (47) for p_{mRNA} in steady state and inserting into (48) gives

$$\frac{dP}{dt} = \alpha_T \kappa_T \left(\frac{\text{TF}^n}{K^n + \text{TF}^n} \right) - \delta_P P \quad (49)$$

with $\alpha_T = \frac{k_l}{\delta_P}$ as the *translation efficiency*. Eq. (49) can further include a constant term κ_B which denotes the *basal transcription rate* at which DNA is transcribed in the absence of up-regulation.

APPENDIX B

DERIVATION OF DYNAMIC LOG-GAIN SENSITIVITY EQUATION

For the derivation of (11) we extend the argumentation resulting in (9) [38]. Eqs. (50a) - (50f) outline the derivation. In (50b) the identity $\frac{\partial \dot{X}_i}{\partial X_j(0)} = 0$ is attributed to $X_j(0)$ not occurring explicitly in \dot{X}_i .

REFERENCES

- [1] T. Nakano, A. W. Eckford, and T. Haraguchi, *Molecular Communication*. Cambridge: Cambridge University Press, 2013.
- [2] L. Felicetti, M. Femminella, G. Reali, and P. Liò, "Applications of molecular communications to medicine: A survey," *Nano Communication Networks*, vol. 7, pp. 27–45, Mar. 2016.
- [3] I. F. Akyildiz, M. Pierobon, S. Balasubramaniam, and Y. Koucheryav, "The internet of Bio-Nano things," *IEEE Communications Magazine*, vol. 53, no. 3, pp. 32–40, Mar. 2015.

$$\frac{d}{dt} \left(\frac{\partial S_{i,X_j(0)}}{\partial \theta_k} \right) = \frac{\partial}{\partial \theta_k} \left(\frac{dS_{i,X_j(0)}}{dt} \right) \quad (50a)$$

$$= \frac{\partial}{\partial \theta_k} \left(\underbrace{\frac{\partial \dot{X}_i}{\partial X_j(0)}}_{=0} \frac{X_j(0)}{X_i} + \underbrace{\frac{\partial X_i}{\partial X_j(0)}}_{=S_{i,X_j(0)} \frac{X_i}{X_j(0)}} \frac{d}{dt} \left(\frac{X_j(0)}{X_i} \right) \right) \quad (50b)$$

$$= \frac{\partial}{\partial \theta_k} \left(\frac{\partial X_i}{\partial X_j(0)} \frac{d}{dt} \frac{X_j(0)}{X_i} \right) \quad (50c)$$

$$= \frac{\partial}{\partial \theta_k} \left(S_{i,X_j(0)} \frac{X_i}{X_j(0)} \right) \frac{d}{dt} \left(\frac{X_j(0)}{X_i} \right) + \frac{\partial X_i}{\partial X_j(0)} \frac{\partial}{\partial \theta_k} \left(\frac{d}{dt} \left(\frac{X_j(0)}{X_i} \right) \right) \quad (50d)$$

$$= \left(\frac{\partial S_{i,X_j(0)}}{\partial \theta_k} X_i + S_{i,X_j(0)} \frac{\partial X_i}{\partial \theta_k} \right) \frac{d}{dt} X_i^{-1} + X_j(0) \frac{\partial X_i}{\partial X_j(0)} \quad (50e)$$

$$= - \left(\frac{\partial S_{i,X_j(0)}}{\partial \theta_k} X_i + S_{i,X_j(0)} \frac{\partial X_i}{\partial \theta_k} \right) \frac{\dot{X}_i}{X_i^2} + X_j(0) \frac{\partial X_i}{\partial X_j(0)} \left(2X_i^{-3} \dot{X}_i - X_i^{-2} \frac{\partial \dot{X}_i}{\partial \theta_k} \right) \quad (50f)$$

- [4] Q. Liu and K. Yang, "Channel capacity analysis of a diffusion-based molecular communication system with ligand receptors," *International Journal of Communication Systems*, vol. 28, no. 8, pp. 1508–1520, 2015.
- [5] S. Mohamed, D. Jian, L. Hongwei, and Z. Decheng, "Molecular communication via diffusion with spherical receiver & transmitter and trapezoidal container," *Microprocessors and Microsystems*, vol. 74, p. 103017, Apr. 2020.
- [6] H. ShahMohammadian, G. G. Messier, and S. Magierowski, "Optimum receiver for molecule shift keying modulation in diffusion-based molecular communication channels," *Nano Communication Networks*, vol. 3, no. 3, pp. 183–195, Sep. 2012.
- [7] H. B. Yilmaz, A. C. Heren, and C.-B. Chae, "3-D Channel Characteristics for Molecular Communications with an Absorbing Receiver," *arXiv:1404.4496 [cs, math, q-bio]*, Apr. 2014.
- [8] M. Veletić, M. T. Barros, I. Balasingham, and S. Balasubramaniam, "A Molecular Communication Model of Exosome-mediated Brain Drug Delivery," in *Proceedings of the Sixth Annual ACM International Conference on Nanoscale Computing and Communication*, ser. NANOCOM '19. New York, NY, USA: Association for Computing Machinery, Sep. 2019, pp. 1–7.
- [9] M. T. Barros, M. Veletic, M. Kanada, M. Pierobon, S. Vainio, I. Balasingham, and S. Balasubramaniam, "Molecular Communications in Viral Infections Research: Modeling, Experimental Data, and Future Directions," *IEEE Transactions on Molecular, Biological and Multi-Scale Communications*, vol. 7, no. 3, pp. 121–141, Sep. 2021.
- [10] M. Kuscü, E. Dinc, B. A. Bilgin, H. Ramezani, and O. B. Akan, "Transmitter and Receiver Architectures for Molecular Communications: A Survey on Physical Design With Modulation, Coding, and Detection Techniques," *Proceedings of the IEEE*, vol. 107, no. 7, pp. 1302–1341, Jul. 2019.
- [11] M. Kuscü, H. Ramezani, E. Dinc, S. Akhavan, and O. B. Akan, "Fabrication and microfluidic analysis of graphene-based molecular communication receiver for Internet of Nano Things (IoNT)," *Scientific Reports*, vol. 11, no. 1, p. 19600, Oct. 2021.
- [12] B. D. Unluturk, A. O. Bicen, and I. F. Akyildiz, "Genetically Engineered Bacteria-Based BioTransceivers for Molecular Communication," *IEEE Transactions on Communications*, vol. 63, no. 4, pp. 1271–1281, Apr. 2015.
- [13] L. Grebenstein, J. Kirchner, W. Wicke, A. Ahmadzadeh, V. Jamali, G. Fischer, R. Weigel, A. Burkovski, and R. Schober, "A Molecular Communication Testbed Based on Proton Pumping Bacteria: Methods and Data," *IEEE Transactions on Molecular, Biological and Multi-Scale Communications*, vol. 5, no. 1, pp. 56–62, Oct. 2019.
- [14] A. Amerizadeh, A. Mashhadian, M. Farahnak-Ghazani, H. Arjmandi, M. A. Rad, A. Shamloo, M. Vosoughi, and M. Nasiri-Kenari, "Bacterial Receiver Prototype for Molecular Communication Using Rhamnose Operon in a Microfluidic Environment," *IEEE Transactions on NanoBioScience*, vol. 20, no. 4, pp. 426–435, Oct. 2021.
- [15] J. R. van der Meer, "Bacterial Sensors: Synthetic Design and Application Principles," *Synthesis Lectures on Synthetic Biology*, vol. 2, no. 1, pp. 1–167, Dec. 2010.
- [16] J. R. van der Meer and S. Belkin, "Where microbiology meets microengineering: Design and applications of reporter bacteria," *Nature Reviews Microbiology*, vol. 8, no. 7, pp. 511–522, Jul. 2010.
- [17] K. Jung, F. Fabiani, E. Hoyer, and J. Lassak, "Bacterial transmembrane signalling systems and their engineering for biosensing," *Open Biology*, vol. 8, no. 4, p. 180023, Apr. 2018.
- [18] R. Tecon and J. R. van der Meer, "Bacterial Biosensors for Measuring Availability of Environmental Pollutants," *Sensors (Basel, Switzerland)*, vol. 8, no. 7, pp. 4062–4080, Jul. 2008.
- [19] Y. Wu, C.-W. Wang, D. Wang, and N. Wei, "A Whole-Cell Biosensor for Point-of-Care Detection of Waterborne Bacterial Pathogens," *ACS Synthetic Biology*, vol. 10, no. 2, pp. 333–344, Feb. 2021.
- [20] M. Woutersen, S. Belkin, B. Brouwer, A. P. van Wezel, and M. B. Heringa, "Are luminescent bacteria suitable for online detection and monitoring of toxic compounds in drinking water and its sources?" *Analytical and Bioanalytical Chemistry*, vol. 400, no. 4, pp. 915–929, 2011.
- [21] A. Struss, P. Pasini, C. M. Ensor, N. Raut, and S. Daunert, "Paper strip whole cell biosensors: A portable test for the semiquantitative detection of bacterial quorum signaling molecules," *Analytical Chemistry*, vol. 82, no. 11, pp. 4457–4463, Jun. 2010.
- [22] C. Miller and J. Gilmore, "Detection of Quorum-Sensing Molecules for Pathogenic Molecules Using Cell-Based and Cell-Free Biosensors," *Antibiotics*, vol. 9, no. 5, p. 259, May 2020.
- [23] D. T. Rıglar and P. A. Silver, "Engineering bacteria for diagnostic and therapeutic applications," *Nature Reviews Microbiology*, vol. 16, no. 4, pp. 214–225, Apr. 2018.
- [24] I. Tanniche and B. Behkam, "Engineered live bacteria as disease detection and diagnosis tools," *Journal of Biological Engineering*, vol. 17, no. 1, p. 65, Oct. 2023.
- [25] H.-J. Chang, P. L. Voyvodic, A. Zúñiga, and J. Bonnet, "Microbially derived biosensors for diagnosis, monitoring and epidemiology," *Microbial Biotechnology*, vol. 10, no. 5, pp. 1031–1035, Aug. 2017.
- [26] J. R. Van Der Meer, D. Tropol, and M. Jaspers, "Illuminating the detection chain of bacterial bioreporters," *Environmental Microbiology*, vol. 6, no. 10, pp. 1005–1020, 2004.
- [27] B. O. Emerenini, B. A. Hense, C. Kuttler, and H. J. Eberl, "A Mathematical Model of Quorum Sensing Induced Biofilm Detachment," *PLOS ONE*, vol. 10, no. 7, p. e0132385, Jul. 2015.
- [28] J. Dockery, "A Mathematical Model for Quorum Sensing in *Pseudomonas aeruginosa*," *Bulletin of Mathematical Biology*, vol. 63, no. 1, pp. 95–116, Jan. 2001.
- [29] A. Meyer, J. A. Megerle, C. Kuttler, J. Müller, C. Aguilar, L. Eberl, B. A. Hense, and J. O. Rädler, "Dynamics of AHL mediated quorum sensing under flow and non-flow conditions," *Physical Biology*, vol. 9, no. 2, p. 026007, Apr. 2012.
- [30] K. Anguige, J. R. King, J. P. Ward, and P. Williams, "Mathematical mod-

- elling of therapies targeted at bacterial quorum sensing.” *Mathematical Biosciences*, vol. 192, no. 1, pp. 39–83, Nov. 2004.
- [31] E. Gustafsson, P. Nilsson, S. Karlsson, and S. Arvidson, “Characterizing the Dynamics of the Quorum-Sensing System in *Staphylococcus aureus*,” *Journal of Molecular Microbiology and Biotechnology*, vol. 8, no. 4, pp. 232–42, Sep. 2005.
- [32] L. Haustenne, G. Bastin, P. Hols, and L. Fontaine, “Modeling of the ComRS Signaling Pathway Reveals the Limiting Factors Controlling Competence in *Streptococcus thermophilus*,” *Frontiers in Microbiology*, vol. 6, 2015.
- [33] T. Ramalho, A. Meyer, A. Mückl, K. Kapsner, U. Gerland, and F. C. Simmel, “Single Cell Analysis of a Bacterial Sender-Receiver System,” *PLOS ONE*, vol. 11, no. 1, p. e0145829, Jan. 2016.
- [34] R. Tecon and J. R. van der Meer, “Information from single-cell bacterial biosensors: What is it good for?” *Current Opinion in Biotechnology*, vol. 17, no. 1, pp. 4–10, Feb. 2006.
- [35] E. O. Voit, “Biochemical Systems Theory: A Review,” *International Scholarly Research Notices*, vol. 2013, p. e897658, Jan. 2013.
- [36] M. A. Savageau, “Introduction to S-systems and the underlying power-law formalism,” *Mathematical and Computer Modelling*, vol. 11, pp. 546–551, Jan. 1988.
- [37] —, “Concepts relating the behavior of biochemical systems to their underlying molecular properties,” *Archives of Biochemistry and Biophysics*, vol. 145, no. 2, pp. 612–621, Aug. 1971.
- [38] R. P. Dickinson and R. J. Gelinias, “Sensitivity analysis of ordinary differential equation systems—A direct method,” *Journal of Computational Physics*, vol. 21, no. 2, pp. 123–143, Jun. 1976.
- [39] F. Shiraishi, Y. Hatoh, and T. Irie, “An efficient method for calculation of dynamic logarithmic gains in biochemical systems theory,” *Journal of Theoretical Biology*, vol. 234, no. 1, pp. 79–85, May 2005.
- [40] J. D. Enderle, “Chapter 7 - Compartmental Modeling,” in *Introduction to Biomedical Engineering (Third Edition)*, ser. Biomedical Engineering, J. D. Enderle and J. D. Bronzino, Eds. Boston: Academic Press, Jan. 2012, pp. 359–445.
- [41] D. K. Button, “Nutrient Uptake by Microorganisms according to Kinetic Parameters from Theory as Related to Cytoarchitecture,” *Microbiology and Molecular Biology Reviews*, vol. 62, no. 3, pp. 636–645, Sep. 1998.
- [42] J. H. Leveau, A. J. Zehnder, and J. R. van der Meer, “The *tfdK* gene product facilitates uptake of 2,4-dichlorophenoxyacetate by *Ralstonia eutropha* JMP134(pJP4),” *Journal of Bacteriology*, vol. 180, no. 8, pp. 2237–2243, Apr. 1998.
- [43] J. R. Van Der Meer, D. Tropel, and M. Jaspers, “Illuminating the detection chain of bacterial bioreporters,” *Environmental Microbiology*, vol. 6, no. 10, pp. 1005–1020, 2004.
- [44] M. H. Zwietering, I. Jongenburger, F. M. Rombouts, and K. van ’t Riet, “Modeling of the Bacterial Growth Curve,” *Applied and Environmental Microbiology*, vol. 56, no. 6, pp. 1875–1881, Jun. 1990.
- [45] M. Peleg, M. G. Corradini, and M. D. Normand, “The logistic (Verhulst) model for sigmoid microbial growth curves revisited,” *Food Research International*, vol. 40, no. 7, pp. 808–818, Aug. 2007.
- [46] JA. Lemos, SR. Palmer, L. Zeng, ZT. Wen, JK. Kajfasz, IA. Freires, J. Abranches, and LJ. Brady, “The Biology of *Streptococcus mutans*,” *Microbiology spectrum*, vol. 7, no. 1, pp. 10.1128/microbiolspec.GPP3-0051–2018, Jan. 2019.
- [47] J. Kaspar, S. A. M. Underhill, R. C. Shields, A. Reyes, S. Rosenzweig, S. J. Hagen, and R. A. Burne, “Intercellular Communication via the comX-Inducing Peptide (XIP) of *Streptococcus mutans*,” *Journal of Bacteriology*, vol. 199, no. 21, pp. e00404–17, Nov. 2017.
- [48] R. Khan, R. Junges, H. A. Åmdal, T. Chen, D. A. Morrison, and F. C. Petersen, “A positive feedback loop mediated by Sigma X enhances expression of the streptococcal regulator ComR,” *Scientific Reports*, vol. 7, no. 1, p. 5984, Jul. 2017.
- [49] M. Iqbal, N. Doherty, A. M. L. Page, S. N. A. Qazi, I. Ajmera, P. A. Lund, T. Kypraios, D. J. Scott, P. J. Hill, and D. J. Stekel, “Reconstructing promoter activity from Lux bioluminescent reporters,” *PLOS Computational Biology*, vol. 13, no. 9, p. e1005731, Sep. 2017.
- [50] S. Hoops, S. Sahle, R. Gauges, C. Lee, J. Pahle, N. Simus, M. Singhal, L. Xu, P. Mendes, and U. Kummer, “COPASI—a COMplex PATHway Simulator,” *Bioinformatics*, vol. 22, no. 24, pp. 3067–3074, Dec. 2006.
- [51] R. Khan, H. V. Rukke, A. P. Ricomini Filho, G. Fimland, M. Ø. Arntzen, B. Thiede, and F. C. Petersen, “Extracellular Identification of a Processed Type II ComR/ComS Pheromone of *Streptococcus mutans*,” *Journal of Bacteriology*, vol. 194, no. 15, pp. 3781–3788, Aug. 2012.
- [52] I. B. Wenderska, A. Latos, B. Pruitt, S. Palmer, G. Spatafora, D. B. Senadheera, and D. G. Cvitkovitch, “Transcriptional Profiling of the Oral Pathogen *Streptococcus mutans* in Response to Competence Signaling Peptide XIP,” *mSystems*, vol. 2, no. 1, pp. 10.1128/msystems.00102–16, Jan. 2017.
- [53] K. Sekar, A. M. Gentile, J. W. Bostick, and K. E. J. Tyo, “N-Terminal-Based Targeted, Inducible Protein Degradation in *Escherichia coli*,” *PLoS ONE*, vol. 11, no. 2, p. e0149746, Feb. 2016.